Annals of Biomedical Engineering, Vol. 42, No. 1, January 2014 *(© 2013)* pp. 50–61
DOI: 10.1007/s10439-013-0898-z

Laser Induced Nitrogen Enhanced Titanium Surfaces for Improved Osseo-Integration

SANKET N. DAHOTRE,[1,3] HITESH D. VORA,[2,3] RAVI SHANKER RAJAMURE,[2,3] LU HUANG,[4] RAJARSHI BANERJEE,[2,3] WEI HE,[4,5] and NARENDRA B. DAHOTRE[2,3]

[1]Texas Academy of Mathematics and Science (TAMS), Denton, TX, USA; [2]Laboratory of Laser Materials Processing and Synthesis, Center for Advanced Research and Technology (CART), Denton, TX, USA; [3]Department of Materials Science and Engineering, University of North Texas, Denton, TX 76203-5017, USA; [4]Department of Materials Science and Engineering, University of Tennessee, Knoxville, TN 37996-2100, USA; and [5]Department of Mechanical, Aerospace and Biomedical Engineering, University of Tennessee, Knoxville, TN 37996-2210, USA

(Received 25 April 2013; accepted 14 August 2013; published online 21 August 2013)

Associate Editor James Tunnell oversaw the review of this article.

Abstract—The osseo-integration, corrosion resistance, and tribological properties of the commonly used bioimplant alloy Ti–6Al–4V were enhanced using a laser-based surface nitridation process. The biomedical properties of the laser nitrided Ti–6Al–4V were investigated using experimental and computational methodologies. Electrochemical analysis of laser nitrided titanium in simulated body fluid (SBF) was performed to assess the biomedical characteristics in near-human body conditions. Additionally, the corrosive wear performance of these laser nitrided samples was evaluated using pin-on-disk geometry with a zirconia pin counter surface in SBF to mimic the biological scenario. Osteoblast studies were conducted to evaluate cell affinity towards titanium nitrided bioimplant material. Cells adhered to all substrates, with high viability. Initial cell adhesion was revealed by focal adhesion formation on all substrates. Cells can proliferate on samples treated with 1.89 and 2.12 $\times$ 10^6 J/m^2 laser conditions, while those treated with 1.70 $\times$ 10^6 J/m^2 inhibited proliferation. Thus, microstructural and phase observations, electrochemical analyses, corrosive wear evaluation, and cell behavior analysis of laser nitrided surface of bioimplant material (Ti–6Al–4V) indicated that laser nitriding greatly improves the performance of bioimplant material.

Keywords—Laser surface nitriding, Laser gas alloying, Laser surface modification, Bioimplants, Osteoblast studies.

INTRODUCTION

Successful implementation of a biomaterial demands that the material be introduced into the human body with required and sufficient biomedical properties to withstand and assimilate itself into a biological surrounding with as few side effects (e.g., allergy, inflammation, toxicity) as possible.[1,3,5] After the biomaterial has been introduced into a biological setting, it must be interpreted, accepted, and integrated by its host as just another part of the biological system.[1] In this respect, after more than 50 years of proven clinical performance and because of excellent biocompatibility, remarkable corrosion resistance, extraordinary strength/weight ratio, high fatigue strength, low elastic modulus, and notable fabricability, Ti and its alloys are the most reliable structural metallic biomaterials over more conventional stainless steels and cobalt-based alloys.[12,16,18,28] Even though titanium for implant fabrication was attempted in the late 1930s, only in 1987 was titanium recognized as potential biomaterial for implant fabrication.[28] However, Ti and its alloys have been just as poorly regarded for their inferior tribological characteristics (abrasive and adhesive wear) as previously reported by many researchers.[26,31,34]

Under the relative sliding at the interface, Ti and its alloys damage the passive (protective) Titanium layer. As a consequence, the release and accumulation of wear debris are among many side effects all-too-common of modern Ti-based implant biomaterials. Such wear debris leads to increased toxicity, which is normally detected by darkened surrounding tissues followed by the mobilization of macrophages that can result in the osteolysis and aseptic loosening of the implant.[26] This often culminates in surrounding tissue reactions and tissue death. Additionally, cells must be

Address correspondence to Narendra B. Dahotre, Department of Materials Science and Engineering, University of North Texas, Denton, TX 76203-5017, USA. Electronic mail: Narendra.Dahotre@unt.edu

able to attach and grow around the Ti-based biomaterial in order to integrate it into the biological system. Without the ability to attach and surround the biomaterials with osteoblast cells (poor osseo-integration), the surrounding tissue will recede from the material, thus requiring immediate revision surgery.[3,5] Therefore, to improve the osseo-integration of Ti-based implant biomaterials in orthopedics, the surface characteristics (surface microstructure and chemistry) must be altered, to enhance tribological characteristics.

In this case, the laser-based surface nitridation process can be an effective solution. During laser surface nitriding, the surface of Ti and its alloys is processed in a nitrogen environment (schematically shown in Fig. 1) that in turn produced titanium nitride (TiN) capable of combatting wear and corrosion.[4,8,13,34] Since the laser beam delivers high energy density confined to the small area in a very short time, such a process in turn generates exceptionally high heating and cooling rates ($>10^5$ K/s) that can produce the unique microstructures with metastable phases or extended solid solubility of nitrogen in Ti, and these microstructures are nearly impossible to achieve from the conventional nitriding methods.

Previously, Sovak *et al.*[26] investigated the performance of TiN layer and validated improved biocompatibility and bone-bonding properties as compared to untreated Ti based alloy (Ti–6Al–4V) implants. Yilbas *et al.*[31] investigated the morphological and metallurgical changes of TiN (titanium nitride) for bioimplants, and found the cracks and micro-void free nitride surface layer. Razavi *et al.*[21,22] determined that TiN based coatings produced by laser gas nitriding dramatically improved electrochemical properties of TiN in HCl. In addition, several experimental and numerical simulation analyses were done to better understand the underlying processes of laser nitriding.[13,24,32] Höche *et al.*[13] carried out several numerical studies by incorporating heat transport, melting effect, diffusion, and convection for synthesis of a TiN surface layer for bioimplants during the laser nitriding process. However, none of these studies (per authors' knowledge) thoroughly investigated the growth characteristics of osteoblasts on laser nitrided substrates and corrosive wear performance of laser nitrided layer in simulated body fluid (SBF), to evaluate biomedical physiognomies in near human body conditions.

In light of this, previously, the present authors developed a multiphysics computational model to mimic the laser nitriding process under various processing conditions and to predict the depth of TiN layer.[10] The evolution of various phases, detailed microstructural investigation, and assessing the concentration of nitrogen were also conducted through X-ray diffraction (XRD), scanning electron microscopy (SEM), and energy dispersive spectroscopy (EDS) observations/analyses, respectively.[10] As both an extension of this work and as part of ongoing incremental efforts, the

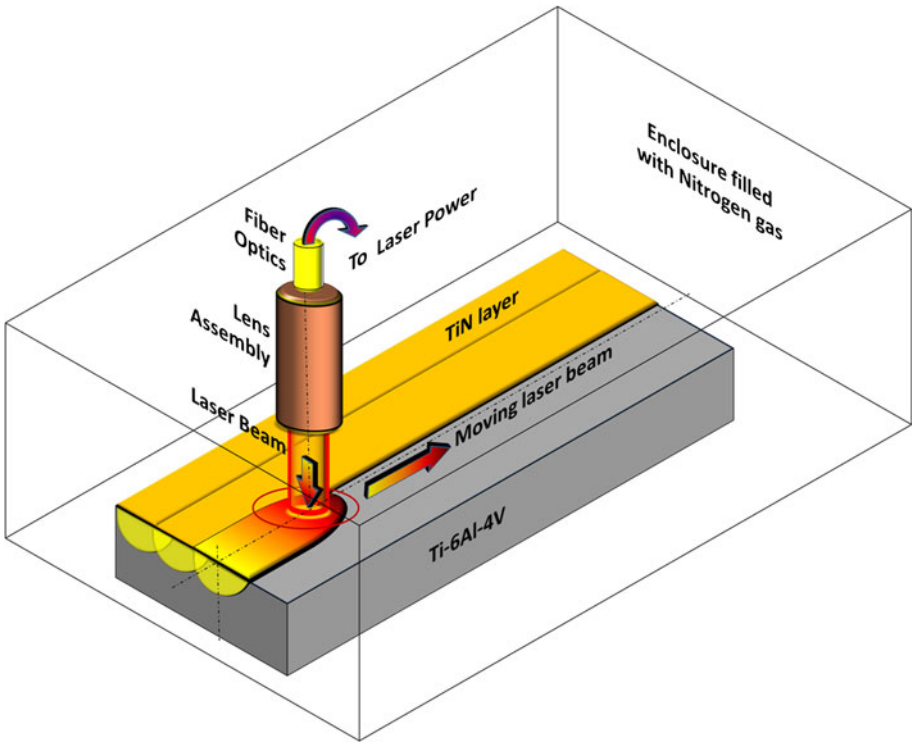

FIGURE 1. Schematic of laser nitriding process.

main objectives of this work were to: (i) explore the corrosive wear characteristics of laser nitrided surface by pin-on-disc sliding in SBF with conditions as similar as possible to orthopedic surgery; (ii) investigate the biomedical characteristics caused by laser nitriding through electrochemical testing; and (iii) study the growth characteristics of osteoblasts on laser nitrided substrates by following the standard procedure previously designed and developed by Huang *et al.*[14] to evaluate biocompatibility.

MATERIALS AND METHODS

Laser Processing

Ti–6Al–4V (alpha–beta titanium alloy, consisting of 6 wt% Al, 4 wt% V, and remaining Ti) coupons ($50 \times 50 \times 3$ mm^3, Trans World Alloys Inc., CA.) was processed using continuous wave mode, Ytterbium laser system (Model # IPG:YLS-3000, 0.6 mm beam diameter, Gaussian TEM_{00} power distribution, 1070 nm wavelength). The coupons were processed inside the processing chamber where nitrogen gas flows continuously at flow rate of 20 L/min at atmospheric pressure. The processing parameters used during laser nitriding are enumerated in Table 1, and a schematic of the experimental setup used in the present work is presented in Fig. 1.

Material Characterization

Electrochemical Testing

The potentiodynamic polarization experiments (*via* anodic polarization) were performed in a standard three-electrode cell consisting of a reference electrode as a saturated calomel electrode (SCE); two parallel graphite rods as a counter electrode; and a coupon as a working electrode. The electrochemical experiments were conducted by exposing a sample area of 1 cm^2. The untreated samples were polished using a series of 600, 800, and 1200 grit SiC sandpapers. Before anodic polarization testing, the coupons were cleaned in an ultrasonic bath using distilled water and air dried. Subsequently, the coupons were mounted in epoxy covering all surfaces except the nitrided surface. The anodic polarization experiments were performed in a stagnant SBF solution at room temperature using a computer controlled potentiostat system (Versa Stat II, EG & G Instruments, Princeton, Oak Ridge, TN).

The electrochemical tests were conducted in SBF at a pH of 7.4 (the pH of human body fluid) to assess the corrosion resistance of laser processed samples in physiological conditions.[33] The SBF was prepared using the following composition: 700 mL H_2O, 8.026 g NaCl, 0.352 g $NaHCO_3$, 0.225 KCl, 0.230 g $K_2HPO_4{\cdot}3H_2O$, 0.311 g $MgCl_2{\cdot}6H_2O$, 0.293 g $CaCl_2$, and 0.0072 g Na_2SO_4.[33] Initial scan was performed by sweeping the potential at a scan rate of 1 mV/s from -250 to $+250$ mV (SCE) in reference to the open circuit potential (OCP). From the anodic polarization plots, the corrosion rate was obtained by means of Tafel extrapolation analysis.[17] To verify consistency of the results, the corrosion experiments were repeated five times.

Corrosive Wear Study

Preliminary wear-corrosion tests were carried out on a pin-on-disc type Tribometer. To replicate the actual orthopedic surgery, the zirconia pin (3 mm diameter and 50 mm long) was specifically chosen for conducting wear-corrosion test.[23,25] The untreated and laser nitrided coupons were clamped on the cylindrical wear cell, which was filled with SBF such that the coupon was totally submerged.[19] The zirconia pin was held stationary under an applied normal load of 0.9 kg while the coupon, which was clamped onto the cylindrical wear cell, was rotating at a speed of 0.0625 m/s using a computer controlled stepper motor. The experiment was conducted in 6 cycles of 2000 rotations each, in order to complete the linear distance of 471 m. The weight losses of pin and coupons after each cycle were measured using a Sartorius digital balance. Further, a total of five readings were taken for each untreated and laser treated coupons (4 coupons $\times$ 5 locations = 20 experiments) to attain higher statistical accuracy in wear-corrosion study.

TABLE 1. Laser processing parameters for laser nitriding.

Laser processing conditions	Nomenclature	1	2	3
Laser power (W)	P		2000 W	
Laser beam diameter (mm)	D		0.6 mm	
Scanning speed (mm/s)	S	2000 mm/s	2250 mm/s	2500 mm/s
Fill spacing (mm)	FS		0.6 mm	
Interaction time (s) $\times 10^{-4}$	$t_r = D/S$	3.00	2.67	2.40
Energy density (J/m^2) $\times 10^6$	$E_g = \left[P/\left(\frac{\pi}{4}D^2\right)\right] t_r$	2.12	1.89	1.7

Roughness and Contact Angle Measurement

Roughness Measurement

The surface roughness measurements were performed using NANOVEA® PS50 optical profilometer with an optical pen of 130 μm at a scanning speed of 1 μm/s. The standard protocol given by the ISO 25178-2:2012 (Geometric Product Specifications–Surface texture: areal) specifications was followed for the surface profile measurements on unprocessed and processed coupons. Furthermore, ISO 4287:1996 standard was utilized for the line profile measurement on the earlier surface profile measurements to estimate the arithmetic average roughness (Ra). The raw data recorded previously during the surface profile measurements was further post-processed by using the NANOVEA® 3D software based on the standard in-built NANOVEA® template. Finally, 12 line-profile measurements were taken to measure the statistically corrected average roughness, Ra (in μm).

Contact Angle Measurement

The CAM-Plus® contact angle goniometer (Cheminstruments, Inc. Fairfield, Ohio) was used for the contact angle measurements by following the patented (US patent 5268733) half angle technique to eliminate inaccuracies related to the arbitrary tangential alignment. A droplet of SBF (~2 mm diameter) was systematically dropped from 22 gauge hypodermic syringe onto the carefully cleaned sample. The 10 contact angle readings at room temperature were taken from random locations after allowing the 10 s droplet stabilization time to reduce statistical errors in the measurement.

Cell Culture and Behaviors

Cell Culture

Laser nitrided samples of each processed condition and untreated sample were cut into $10 \times 10 \times 3$ mm^3 coupons. The samples were ultrasonically cleaned in acetone, ethanol, and deionized water for 5 min each, followed by overnight UV exposure to achieve sterilization. Mouse MC3T3-E1 pre-osteoblasts were incubated in a growth medium (alpha minimum essential medium +10% fetal bovine serum +1% penicillin–streptomycin) in a 5% CO_2 balanced air incubator maintained at 37°C. Confluent cells were removed using 0.25% trypsin with ethylenediaminetetraacetic acid (EDTA) and re-suspended in fresh culture medium for cellular behavior studies. Cells were seeded on triplicate samples at a density of 5×10^3 cells/cm^2 for each characterization.

Cell Viability and Attachment

Cell attachment and viability studies were carried out using a live/dead staining assay (Invitrogen, USA). After 4 h of growth, cells on each sample were stained simultaneously with calcein AM (2 μm) to identify viable cells and ethidium homodimer-1 (EthD-1; 4 μm) to distinguish non-viable cells. A semi-quantitative analysis was carried out on the fluorescent images by manually counting the cell numbers by three randomly selected areas (~0.56 mm^2) per sample.

Cell Morphology

Cell morphology after 4 h of growth was visualized *via* SEM to reveal the initial cell interactions with the substrates. Briefly, cultured cells were fixed with 3% glutaraldehyde and dehydrated using serial dehydration with increasing ethanol grades (from 25 to 50 to 75 to 95 to 100%). Chemical dehydration was performed to further remove water, with the mixture of ethanol and hexamethyl disilazane (HMDS) (2:1, 1:1, and 1:2), followed by immersion twice in 100% HMDS. Samples were then stored in vacuum desiccator to allow complete evaporation of HMDS and, finally, were kept in vacuum until imaging. SEM images of gold coated samples were collected in secondary electron (SE) mode at 5 kV using LEO 1525 scanning electron microscope (LEO Electron Microscopy, Germany).

Focal Adhesion Formation and Actin Cytoskeleton Development

The formation of focal adhesion and development of actin cytoskeleton was viewed with fluorescent staining of the vinculin and actin filaments. After incubation (4 h), the cells were fixed in 4% paraformaldehyde, permeabilized using 0.1% Triton X-100 (Sigma, USA), and blocked using 1% bovine serum albumin (Sigma, USA). The intracellular vinculin was labeled with a primary vinculin monoclonal antibody (2 μg/mL, Chemicon, USA) followed by a secondary antibody, Alexa fluor 488 goat anti-mouse IgG1 (Invitrogen, USA). Actin filaments were then labeled with Alexa fluor 594-conjugated phalloidin (40 μg/mL). Cell nuclei were stained with 4′,6-Diamindino-2-phenylindole (DAPI, Chemicon, USA).

Cell Proliferation

Cell proliferation behaviors were evaluated using WST-1 assay (Roche Applied Science, USA) 1, 3, and 5 days after seeding on triplicate samples. This assay involves a water soluble tetrazolium salt as the reagent, which will be reduced to formazan by mitochondrial dehydrogenase. Therefore, the spectrophotometrical

quantification of formazan can be directly associated with the number of viable cells and their metabolic activities. The absorbance of the product was measured at 440 nm using Synergy 2 Multi-Mode Microplate Reader (Biotek, USA).

Statistical Analyses

All measured data are reported in terms of mean ± standard deviation. Student's *t* test was performed on each group of data in comparison with the reference data obtained on untreated samples. A *p*-value less than 0.05 was considered statistically significant (denoted by asterisks).

RESULTS AND DISCUSSIONS

Phase and Microstructural Analysis

Based on the previous studies, the XRD analyses revealed the presence of titanium nitride (δ-TiN, face-centered cubic based NaCl structure) and α-Ti phases in the surface and subsurface regions of the laser nitrided samples processed with various laser energy density (1.70, 1.89, and 2.12×10^6 J/m^2).[10] In addition, based on the relative intensity ratio, (111) δ-TiN peak divide by (10$\bar{1}$1) α-Ti peak, the volume fraction of the δ-TiN phase proportionally increased (5.3 to 7.3 to 9.5%) with an increase in laser energy density (1.70 to 1.89 to 2.12×10^6 J/m^2.[10] Furthermore, SEM analysis on the cross section of all laser nitrided samples confirmed the formation of TiN layer. During laser nitriding treatment, the inherent characteristics of the laser beam generate higher heating and cooling rates on the sample surface enclosed in a nitrogen filled chamber and influence the formation of three distinct layers/zones, starting from top to bottom; namely nitride layer, heat affected zone, and Ti–6Al–4V base material, respectively (Fig. 2). The depth of the nitride layer was experimentally measured from the SEM backscattered electron images of the laser treated sample. During this analysis, the nitride layer depth systematically increased (from 9.5 to 11.3 to 13.8 μm) with an increase in average energy density (1.70 to 1.89 to 2.12×10^6 J/m^2).[10] Additional details about phase evolution, microstructural analyses, and experimental observations during laser nitriding are provided elsewhere.[10]

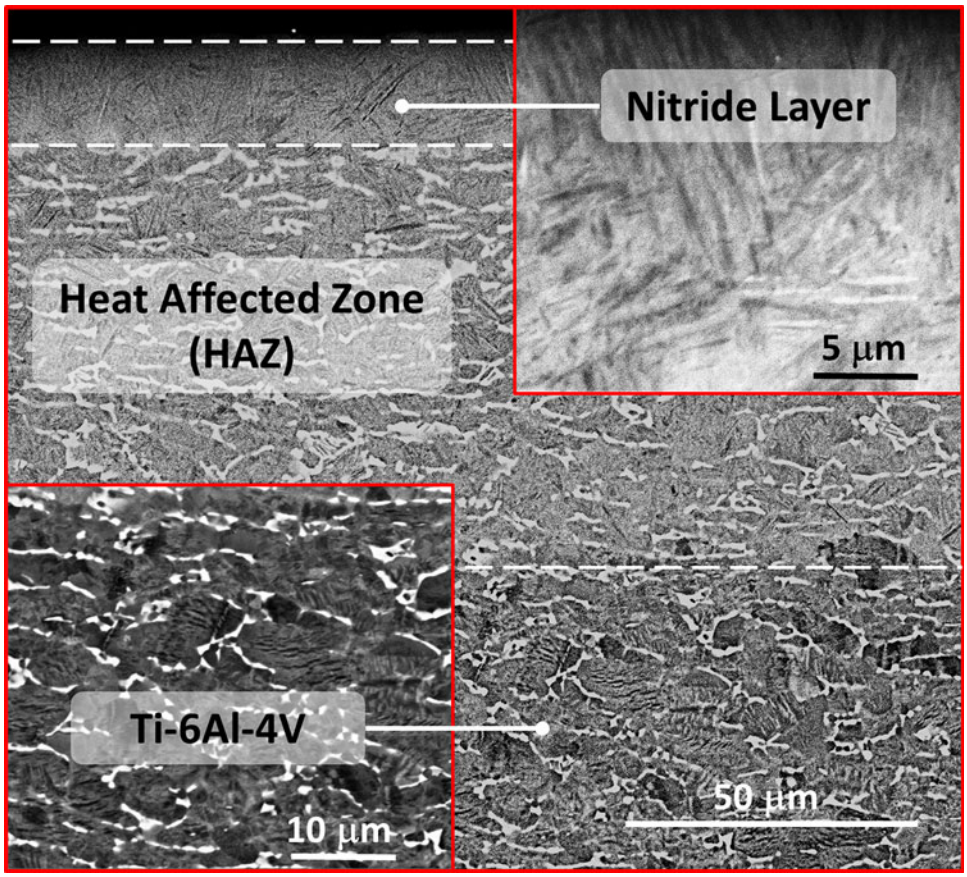

FIGURE 2. Evolution of microstructures during laser nitriding of Ti–6Al–4V (1.89×10^6 J/m^2 laser energy density).

Electrochemical Behavior

Electrochemical analysis of the nitrided samples compared with base Ti–6Al–4V (alpha–beta titanium alloy) indicated a remarkable effect of nitriding on corrosion resistance (Fig. 3). The findings from the electrochemical experiments in SBF solution clearly elucidated (Fig. 3a) that untreated Ti–6Al–4V corrodes at a considerably lower corrosion potential (−477 mv (SCE)), which is indicative of a high corrosion rate (Fig. 3b). This can be attributed to the presence of defects such as the existence of imperfections within the crystal lattice, residual impurities, and microstructure (physical or chemical) inhomogeneities such as intermetallic precipitates.[11,27] High volume pit formation on the surface (Fig. 4a) of the untreated Ti–6Al–4V clearly indicated localized pitting corrosion and is attributed mainly to micro-galvanic coupling among the alloying elements (Al, V) present in the form of solid solution alpha (Al rich) and beta (V rich) phases, which displayed the anodic behavior with the matrix (Ti rich). The high corrosion rate of the untreated samples can also be attributed to the uneven segregation of alloying elements, leading to increased galvanic coupling.

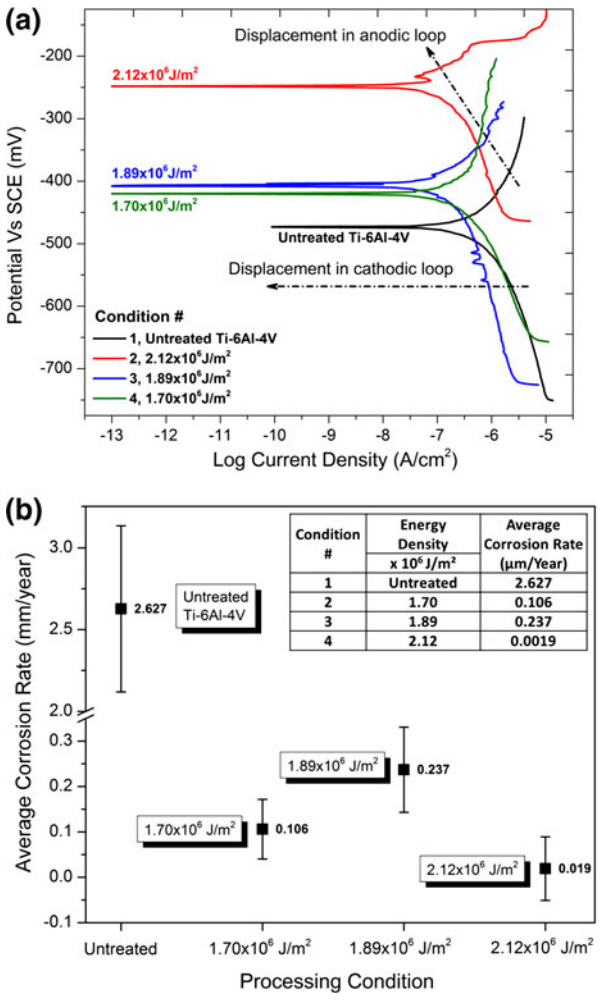

FIGURE 3. Corrosion analysis. (a) potentiodynamic response, and (b) corrosion rate for various laser processing conditions.

Comparison of laser treated and untreated samples corroborated a substantial enhancement in corrosion resistance due to the formation of titanium nitride (TiN), a highly inert phase (Fig. 3b).[21] The substantial improvement in corrosion resistance was due mainly to the shift in the corrosion potential (−477 to −244 mv) in a nobler direction (Fig. 3a). Additionally, the presence of TiN in the passive film substantially modified electrochemical properties, resulting in a high resistance to corrosion. This was clearly evidenced in the shift of the anodic loop towards a nobler direction after laser nitriding (Fig. 3a). Moreover, the rapid heating and cooling inherently associated with the laser processing achieved a homogeneous phase transformation on laser nitrided samples that resulted in uniform dissolution of alloying elements (Al, V), and promoted the formation of TiN solid solution on the surface. This results in the chemical homogeneity that led to relatively low levels of uniform corrosion and reduced corrosion attack across the surface of the substrate (Figs. 4b, 4c, 4d); hence, a substantial decrease in the overall corrosion rate (Fig. 3b). Electrochemical studies of laser nitrided titanium in SBF have, to the best of the authors' knowledge, never before been conducted.

Corrosive Wear

The corrosive wear response at the end of 12,000 revolutions (6 cycles of 2000 revolution) of untreated and laser nitrided samples is presented in Fig. 5a. In addition, the maximum cumulative wear rate of 8.17 mg/mm^2/12,000 revolutions (Fig. 5b) was observed for untreated Ti–6Al–4V sample compared to all laser nitrided samples. However, a previous observation was that with an increase in laser energy density, the depth of the nitride layer also increased, which in turn decreased the wear rate (3.05 to 1.94 to 1.16, Fig. 5b). The average maximum depths of wear track obtained along the wear track for untreated and laser treated samples are enumerated in Table 2. These data clearly indicate better corrosive wear resistance with the lowest wear track depth of 6.68 μm for the sample that was laser processed at 2.12 $\times$ 10^6 J/m^2 (Fig. 3 and Table 2) thus further confirming the results of wear rate (Fig. 5). This enhancement in the wear response after laser nitriding directly corroborated with the modification in microstructure as well as electrochemical response of the nitrided surface.

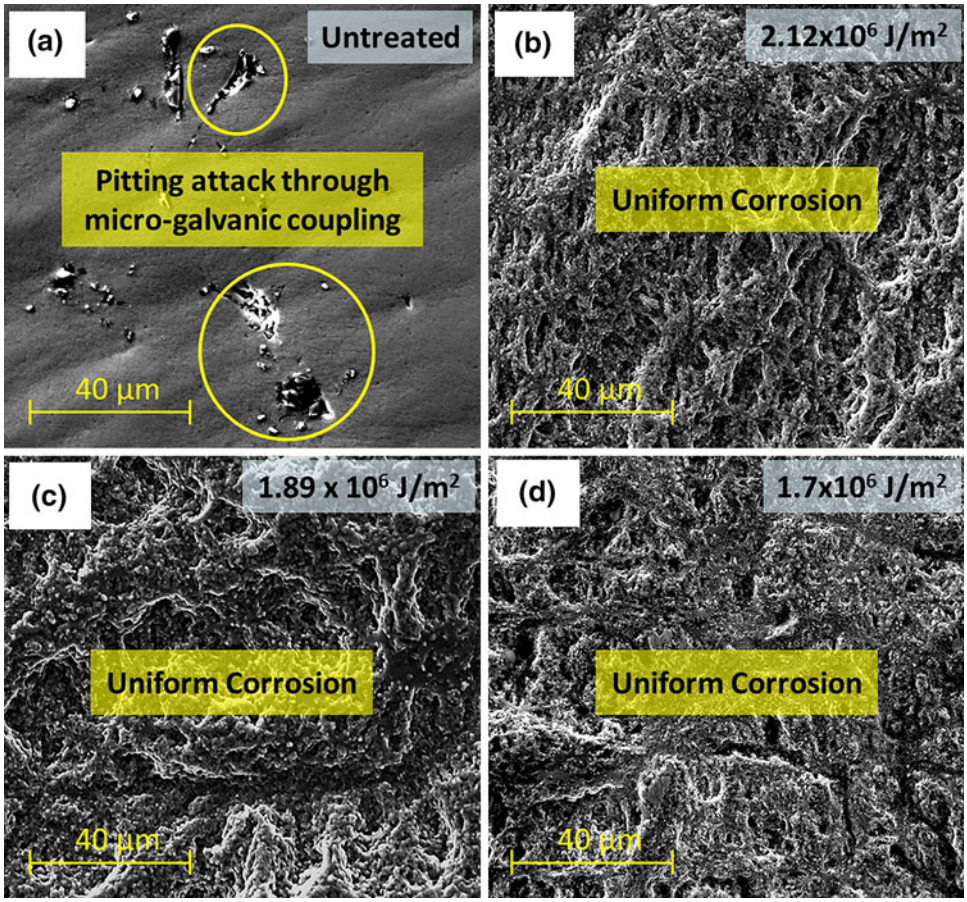

FIGURE 4. SEM micrographs of surface morphology after electrochemical testing (a) untreated sample, (b) 2.12 × 10^6 J/m^2, (c) 1.89 × 10^6 J/m^2, and (d) 1.70 × 10^6 J/m^2.

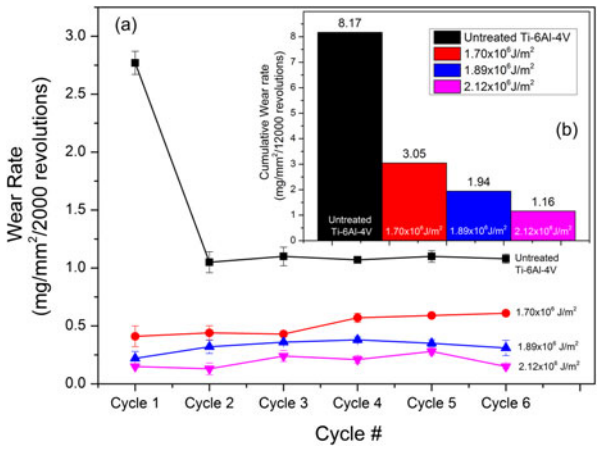

FIGURE 5. Corrosive wear response (a) wear rate as function of revolutions, and (b) cumulative wear rate as function of laser input energy.

Cellular Behavior Analysis

Initial Cell Attachment, Viability, and Morphology

Live/dead staining results (Fig. 6) indicated that all substrates were capable of supporting the initial attachment of MC3T3-E1 cells within 4 h of incubation. The few dead or disrupted cells suggested good initial adhesion and very high viability of cells on both the laser nitrided surfaces and the untreated coupons. Semi-quantification on the number/density of the adherent cells indicates that the numbers of cells attached on the surfaces treated under 2.12 × 10^6 and 1.89 × 10^6 J/m^2 were comparable with the control. However, cell density on the surface treated with the lowest laser energy (1.70 × 10^6 J/m^2) was significantly lower than that of the control. Differences in initial cell attachment between untreated samples and nitrided samples can be attributed to the changes of many different surface factors including the change in surface chemistry, increase in surface roughness (Fig. 7a), and decrease in hydrophilicity (Fig. 7b). Given that the surface chemistry on laser treated samples was nearly identical, cell attachment behaviors on treated samples were analyzed by correlating with surface wettability. Surface wettability is known to affect protein adsorption, which conditions the surface and modulates cell adhesion.[7] In the current study, increasing energies in laser nitriding from 1.70 × 10^6 J/m^2 to 2.12 × 10^6 J/m^2

TABLE 2. Average maximum depth of wear track.

Condition #	Laser energy density $\times 10^6$ J/m^2	Average maximum depth of wear track (μm)
1	Untreated	37.1
2	1.70	18.4
3	1.89	12.1
4	2.12	6.68

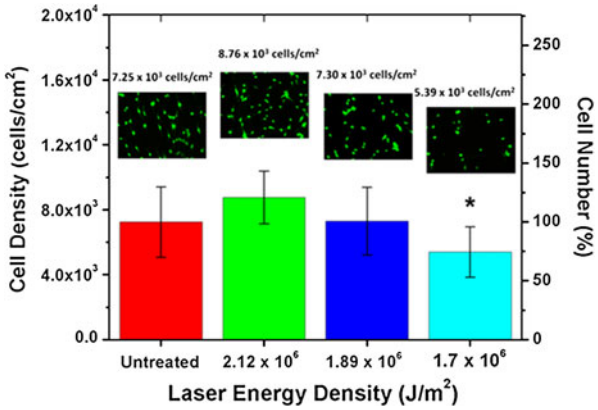

FIGURE 6. Variation in cell density and cell numbers under different laser processing conditions. The cell numbers are represented with respect to untreated sample. $p < 0.05$ are considered to be strategically significant and are denoted by *.

and 1.89 $\times$ 10^6 J/m^2 introduced a general increase in contact angle from around 63° to around 75° (Fig. 7b), which can be directly related to higher numbers of adherent cells on 2.12 $\times$ 10^6 J/m^2 and 1.89 $\times$ 10^6 J/m^2 treated samples. Although this simple relationship between wettability and adherent cells is effective in the current study, other surface factors are important to modulation of cell adhesion. In fact, surface properties, protein adsorption and cellular behaviors can be mutually correlated and influence each other,[20,29] and would require a more in-depth study.

As shown in the SEM images in Fig. 8, cell morphology was sensitive to the surface topography introduced by laser nitriding. On the smooth control surface, cells were randomly distributed, with a large number of the population spreading out extensively on the surface. In contrast, the micron sized surface features of laser treated surfaces caused polarization of adherent cells. Additionally, preferential orientation towards grooves formed by the overlapping of laser tracks was observed on treated samples. Such a selective interaction could be due to the physical feature or the chemical composition of the surface, or a combination of both.[15] A detailed discussion on the underlying mechanism requires further investigations.

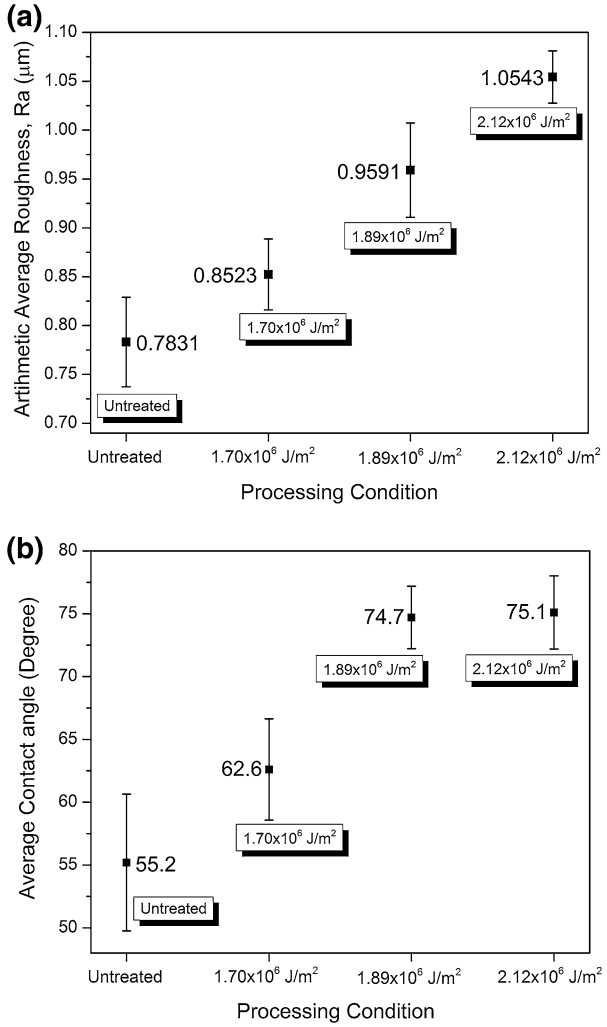

FIGURE 7. Surface characteristics (a) surface roughness as function of laser input energy, and (b) contact angle as function of laser input energy.

Surface nitriding effects on cell adhesion were studied by examining the focal adhesion and F-actin cytoskeleton of the cells (Fig. 9). The development of cytoskeleton system and the formation of focal adhesion can be clearly observed on all specimens. On untreated samples, cells were extensively spread over the surface showing polygonal shapes, which are in agreement with the SEM observation described above. The focal adhesion plaques on the periphery of the cytoplasm and the actin filament bundles were formed in various directions, mainly along cell periphery and sometimes circulating the cytoplasm. On nitrided samples, cells were preferentially oriented, and focal adhesion plaques can be recognized on the polar ends of the elongated cells. Actin filaments were also strongly directed and ran parallel to the cell axes. Qualitatively, fewer focal adhesion plaques (shown by the strong green-positive signals, Fig. 9) can be determined for those polarized cells found on nitriding

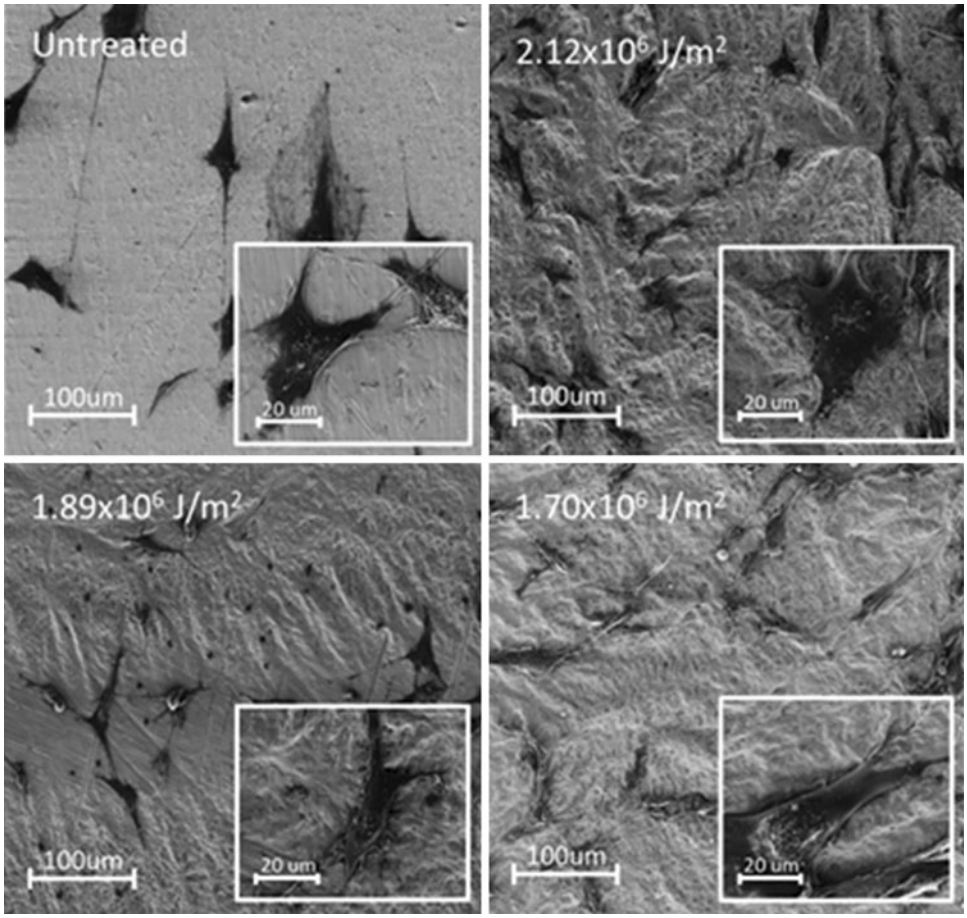

FIGURE 8. SEM secondary electron images for cell morphology on the different substrates after 4 h seeding.

treated samples as compared to those well-extended cells on untreated samples. The significance of cell adhesion lies in its direct impact on cell mobility, which can be correlated with other cell functions including proliferation and differentiation. Also worth noting is that surface nitriding introduced deformation of cell nuclei to MC3T3-E1 cells, as can be clearly observed in the insets in Fig. 9. The cell nuclei on untreated samples were round-shaped, while those on treated samples were elliptic-shaped and were aligned along the long axes of cells. The deformation in cell nuclei may influence the downstream differentiation behaviors and gene expression.[9,30]

Cell Proliferation

Cell proliferation behaviors on different substrates at various time points up to 5 days were monitored using WST-1 assay as shown in Fig. 10. The number of cells is directly proportional to absorbance. The proliferation rates of MC3T3-E1 cells can be evaluated by the slope of the curves from Fig. 11. Cell proliferation on surfaces with the lowest energy (1.70×10^6 J/m^2) laser nitriding treatment was inhibited, as presented by the unchanged absorbance from day 1 to day 5 (Fig. 10). A slight cell growth was observed on 1.70×10^6 J/m^2 treated samples from day 1 to day 3, followed by a decrease in the number of cells from day 3 to day 5, as depicted by the negative slope of the growth curve (Fig. 11). In contrast, cells attached on the surfaces treated with higher laser energies (2.12×10^6 and 1.89×10^6 J/m^2) were metabolically active and proliferating, as confirmed by the increasing absorbance with incubation time. Higher cell number and proliferation rate were found on 2.12×10^6 J/m^2 treated samples as compared to 1.89×10^6 J/m^2 treated surfaces from day 1 to day 3, which then became equivalent from day 3 to day 5. Surface chemistry could be one of factor that affected cell proliferation behavior and led to the inhibition of cell growth on 1.70×10^6 J/m^2 treated surfaces. Significant reduction in cell viability and proliferation were found for certain surface nitriding treatment to Ti alloys,[6] although other studies found no significant difference in cell behaviors with and without nitriding.[2] In the meantime, other components ((i.e., surface roughness

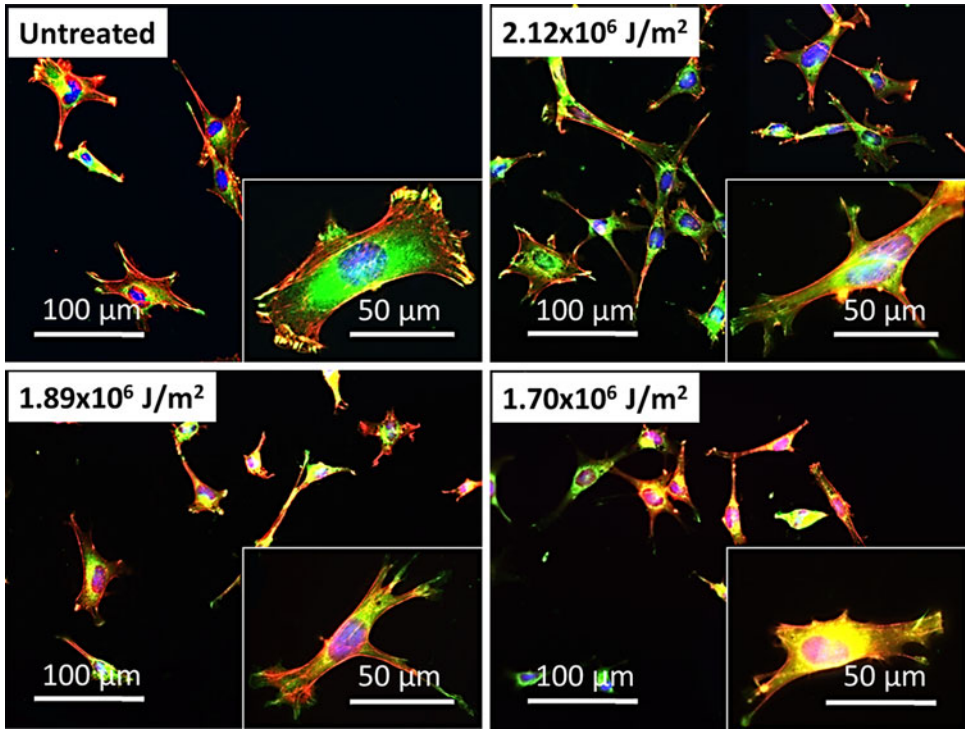

FIGURE 9. Fluorescent images taken for MC3T3-E1 cells adherent on the different substrates after 4 h, showing focal contacts (green), actin filaments (red) and the nucleus (blue).

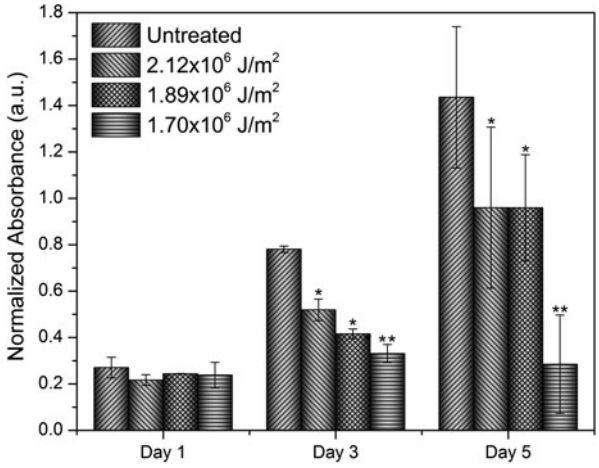

FIGURE 10. WST-1 assay results representing proliferation activities of MC3T3-E1 cells after 1, 3, and 5 days of growth. $p < 0.05$ are considered to be strategically significant and are denoted by *.

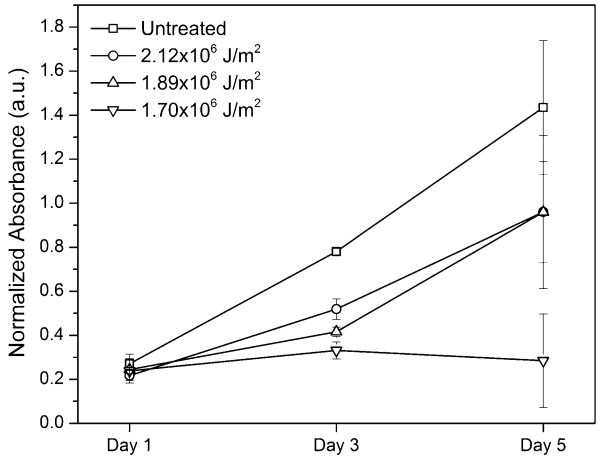

FIGURE 11. Proliferation rates of MC3T3-E1 cells on different substrates.

(Fig. 7a), surface morphology/features)) may also contribute to proliferation behaviors. Highest absorbance was found for untreated samples at all-time points. However, the growth rate of MC3T3-E1 cells on 2.12×10^6 and 1.89×10^6 J/m^2 treated surfaces was equivalent to that on untreated samples from day 3 to day 5. Such extensive cell study (cell attachment, viability, morphology, and proliferation studies) on nitrided Ti–6Al–4V bioimplant material has, to the best of the authors' knowledge, been conducted for the first time.

CONCLUSION

A laser based surface modification technique was successfully used on nitride Ti–6Al–4V bioimplant material for improved biomedical properties. Electrochemical

analysis indicated a remarkable increase in corrosion resistance after laser nitriding. Untreated Ti–6Al–4V samples showed a corrosion rate of 2.627 μm/year while after nitriding samples of laser energy densities of 1.70, 1.89, and 2.12 $\times$ 10^6 J/m^2 showed corrosion rates of 0.019, 0.237, 0.106 μm/year, respectively. The corrosive wear analysis also evidently revealed the decrease in wear rate (3.05, 1.94, 1.16 mg/mm^2/12,000 revolutions) of laser treated sample processed with an increase in laser energy densities of 1.70, 1.89, and 2.12 $\times$ 10^6 J/m^2, respectively. Cellular behavior analysis determined that cells seeded on samples treated with laser energy density of 1.89 and 2.12 $\times$ 10^6 J/m^2 had viability comparable to that of the control, while cells seeded on samples treated with laser energy density of 1.70 $\times$ 10^6 showed viability significantly lower than that of the control. Laser nitriding-induced morphological changes to MC3T3-E1 cells include change in cell shapes and orientation, distribution and amount of focal adhesion plaques, alignment of actin filaments, and shape of nuclei. Cell proliferation studies indicated that cells grown on samples treated with the highest laser energy densities (1.89 and 2.12 $\times$ 10^6 J/m^2) were metabolically active, while absorbance of cells grown on samples treated with the lowest laser energy density (1.70 $\times$ 10^6 J/m^2) was inhibited. Cell growth rates from day 3 to day 5 on samples treated with higher laser energy were comparable to those on untreated samples. Previous and present studies as well as microstructural and phase observations, corrosion evaluation, and cell behavior analysis of laser nitrided surface of bioimplant material (Ti–6Al–4V) confirm that laser based surface treatment is highly effective in treating bioimplant material for improved performance in physiological environments. Further, due to its unique physical and optical characteristics, the laser lends itself to precise, rapid, and automated processing of bioimplants.

As little research on the biomedical applications of titanium nitride has been conducted, the results in this paper are not easily compared. Therefore, the conclusions reported are based solely on evidence provided through experimentation conducted by the authors. In light of this, results observed in this research show laser nitrided titanium to demonstrate the qualities necessary for biomedical applications. Titanium nitride has the potential to be a next-generation biomaterial capable of increasing the lifespan and efficiency of modern day implants. To refine this conclusion, the goal of the present research is to examine the effects of titanium nitride implants on a human implant simulator. Using this equipment would provide further insight into biomedical properties of titanium nitride that cannot be realistically measured in a laboratory setting.

ACKNOWLEDGMENTS

The authors appreciate Iman Ghamarian, Vasim Shaikh, Yee-Hsien Ho, and Pavani Kami for their help in experimental investigations especially for SEM, XRD, surface roughness and contact angle measurements. Availability of the characterization facility in the Center for Advanced Research Technology (CART) at the University of North Texas is acknowledged.

REFERENCES

[1]Albrektsson, T., and C. Johansson. Osteoinduction, osteoconduction and osseointegration. *Eur. Spine J.* 10:96–101, 2001.

[2]Annunziata, M., L. Guida, L. Perillo, R. Aversa, I. Passaro, and A. Oliva. Biological response of human bone marrow stromal cells to sandblasted titanium nitride-coated implant surfaces. *J. Mater. Sci. Mater. Med.* 19:3585–3591, 2008.

[3]Basu, B., D. Katti, and A. Kumar. Advanced Biomaterials: Fundamentals, Processing, and Applications. Hoboken, N.J.; [Westerville, Ohio]: John Wiley & Sons; The American Ceramic Society, 2009.

[4]Biswas, A., T. K. Maity, U. K. Chatterjee, I. Manna, L. Li, and J. D. Majumdar. Laser surface nitriding of Ti–6Al–4V for bio-implant application. *Lasers Eng.* 17:59–73, 2006.

[5]Black, J. Biological Performance of Materials: Fundamentals of Biocompatibility. New York: Taylor & Francis Group, 2006.

[6]Bordji, K., J. Y. Jouzeau, D. Mainard, E. Payan, P. Netter, K. T. Rie, T. Stucky, and M. Hage-Ali. Cytocompatibility of Ti-6Al-4V and Ti-5Al-2.5Fe alloys according to three surface treatments, using human fibroblasts and osteoblasts. *Biomaterials* 17:929–940, 1996.

[7]Boyan, B. D., T. W. Hummert, D. D. Dean, and Z. Schwartz. Role of material surfaces in regulating bone and cartilage cell response. *Biomaterials* 17:137–146, 1996.

[8]Chung, K. H., G. T. Liu, J. G. Duh, and J. H. Wang. Biocompatibility of a titanium–aluminum nitride film coating on a dental alloy. *Surf. Coat. Technol.* 188–189: 745–749, 2004.

[9]Curtis, A. S. G. Mechanical tensing of cells and chromosome arrangement. In: Biomechanics and Cells, edited by F. Lyall and A. J. El Haj. Cambridge: Cambridge University Press, 1994, pp. 121–130.

[10]Dahotre, S. N., H. D. Vora, K. Pavani, and R. Banerjee. An integrated experimental and computational approach to laser surface nitriding of Ti–6Al–4V. *Appl. Surf. Sci.* 271:141–148, 2013.

[11]Davis, J. R. Corrosion: Understanding the Basics. ASM International, 2000.

[12]Donachie, M. J. Titanium: A Technical Guide. Materials Park, OH: ASM International, 2000.

[13]Höche, D., and P. Schaaf. Laser nitriding: investigations on the model system TiN. A review. *Heat Mass Transf.* 47:519–540, 2011.

[14]Huang, L., Z. Cao, H. M. Meyer, P. K. Liaw, E. Garlea, J. R. Dunlap, T. Zhang, and W. He. Responses of bone-forming cells on pre-immersed Zr-based bulk metallic

glasses: effects of composition and roughness. *Acta Biomater*. 7:395–405, 2011.
[15]Kilian, K. A., B. Bugarija, B. T. Lahn, and M. Mrksich. Geometric cues for directing the differentiation of mesenchymal stem cells. *Proc. Natl. Acad. Sci. USA* 107(11):4872–4877, 2010.
[16]Lütjering, G., and J. C. Williams. Titanium. Berlin: Springer, 2007.
[17]McCafferty, E. Validation of corrosion rates measured by the Tafel extrapolation method. *Corros. Sci*. 47:3202–3215, 2005.
[18]Oshida, Y. Bioscience and bioengineering of titanium materials. The Boulevard, Langford Lane, Kidlington, Oxford OX5 1GB, UK: Elsevier, 2007.
[19]Paital, S. R., and N. B. Dahotre. Wettability and kinetics of hydroxyapatite precipitation on a laser-textured Ca–P bioceramic coating. *Acta Biomater*. 5:2763–2772, 2009.
[20]Ratner, B. D. Biomaterials Science an Introduction to Materials in Medicine. San Diego, CA: Academic Press, 2004.
[21]Razavi, R. S., G. R. Gordani, and H. C. Man. A review of the corrosion of laser nitrided Ti–6Al–4V. *Anti-Corros. Methods Mater*. 58(3):140–154, 2011.
[22]Razavi, R. S., M. Salehi, M. Monirvaghefi, and R. Mozafarinia. Effect of laser gas nitriding on the microstructure and corrosion properties of Ti–6Al–4V alloy. *ISIJ Int*. 47:709–714, 2007.
[23]Ruff, A. W. Wear measurements. In: ASM Handbook on Friction, edited by S. D. Henry. Materials Park, OH: Lubrication and Wear Technology, pp. 362–369, 1998.
[24]Schaaf, P. Laser nitriding of metals. *Prog. Mater Sci*. 47:1–161, 2002.
[25]Singh, R., A. Kurella, and N. B. Dahotre. Laser surface modification of Ti–6Al–4V: wear and corrosion characterization in simulated biofluid. *J. Biomater. Appl*. 21:49–73, 2006.
[26]Sovak, G., A. Weiss, and I. Gotman. Osseointegration of Ti6Al4V alloy implants coated with titanium nitride by a new method. *J. Bone Joint. Surg. Br*. 82:290–296, 2000.
[27]Szklarska-Smialowska, Z. National Association of Corrosion Engineers. Pitting Corrosion of Metals. Houston, TX: National Association of Corrosion Engineers, 1986.
[28]Van Noort, R. Titanium: the implant material of today. *J. Mater. Sci*. 22:3801–3811, 1987.
[29]Yang, Y., R. Cavin, and J. L. Ong. Protein adsorption on titanium surfaces and their effect on osteoblast attachment. *J. Biomed. Mater. Res. A* 67:344–349, 2003.
[30]Yang, J., Y. Ting, J. Lai, H. Liu, H. Fang, and W. Tsai. Quantitative analysis of osteoblast-like cells (MG63) morphology on nanogrooved substrata with various groove and ridge dimensions. *J. Biomed. Mater. Res. A* 90:629–640, 2009.
[31]Yilbas, B. S., C. Karatas, B. Ersu, and S. Gurgan. Laser gas-assisted nitriding of Ti implant. *Ind. Lubr. Tribol*. 63:4:293–302, 2011.
[32]Yilbas, B. S., S. Z. Shuja, and M. S. J. Hashmi. A numerical solution for laser heating of titanium and nitrogen diffusion in solid. *J. Mater. Process. Technol*. 136:12–23, 2003.
[33]Zaveri, N. A. Biocorrosion Studies of Surface Modified Bioimplant Materials in Simuated Body Fluids. Logan, UT: Utah State University, 2007.
[34]Zhecheva, A., W. Sha, S. Malinov, and A. Long. Enhancing the microstructure and properties of titanium alloys through nitriding and other surface engineering methods. *Surf. Coat. Technol*. 200:2192–2207, 2005.